



**HAL**  
open science

## Co-pyrolysis of beech wood and polyamide-6: Effect of HZSM-5 catalyst on the properties of pyrolysis oils

William de Rezende Locatel, Chetna Mohabeer, Dorothee Laurenti, Y. Schuurman, Nolven Guillaume

### ► To cite this version:

William de Rezende Locatel, Chetna Mohabeer, Dorothee Laurenti, Y. Schuurman, Nolven Guillaume. Co-pyrolysis of beech wood and polyamide-6: Effect of HZSM-5 catalyst on the properties of pyrolysis oils. *Journal of Analytical and Applied Pyrolysis*, 2022, 167, pp.105696. 10.1016/j.jaap.2022.105696 . hal-04287953

**HAL Id: hal-04287953**

**<https://hal.science/hal-04287953>**

Submitted on 15 Nov 2023

**HAL** is a multi-disciplinary open access archive for the deposit and dissemination of scientific research documents, whether they are published or not. The documents may come from teaching and research institutions in France or abroad, or from public or private research centers.

L'archive ouverte pluridisciplinaire **HAL**, est destinée au dépôt et à la diffusion de documents scientifiques de niveau recherche, publiés ou non, émanant des établissements d'enseignement et de recherche français ou étrangers, des laboratoires publics ou privés.

1 **Co-pyrolysis of beech wood and polyamide-6: Effect of HZSM-5 catalyst on the properties**  
2 **of pyrolysis oils**

3 William de Rezende Locatel, Chetna Mohabeer, Dorothee Laurenti, Yves Schuurman, Nolven  
4 Guillaume\*

5 Univ. Lyon, Université Claude Bernard Lyon 1, CNRS, IRCELYON – UMR 5256, 2 Avenue  
6 Albert Einstein, F-69626 Villeurbanne Cedex, France

7 \* Corresponding author, [nolven.guilhaume@ircelyon.univ-lyon1.fr](mailto:nolven.guilhaume@ircelyon.univ-lyon1.fr)

8  
9 **Abstract**

10 Biomass residues and waste can be converted into bioliquids by pyrolysis, which can contribute to  
11 both the production of renewable fuels and the recycling of waste. In this paper, the pyrolysis of  
12 pure beech wood (BW) and of a mixture of BW + polyamide-6 (PA6), a nitrogen-containing  
13 plastic, was investigated to assess the effect of PA6 on the properties of bio-oils, obtained either  
14 by thermal pyrolysis or by pyrolysis with ex-situ catalytic treatment of the vapors. The presence  
15 of 20 wt.% PA6 in the blend affected the pyrolysis products yields and distribution (gases, liquids,  
16 chars), but also the composition of the bioliquids. In absence of a catalyst, the production of  
17 phenolic compounds (guaïacol, syringol...), sugars, furans decreased significantly with the  
18 BW+PA6 blend compared to pure BW, and N-containing compounds derived from PA6 were  
19 found in the bioliquids. When HZSM-5 catalyst was applied for the treatment of vapors, a  
20 beneficial effect of the catalyst on the reduction of the sugars and furans content in the bioliquids  
21 and on the production of deoxygenated compounds was observed with pure BW. This effect was  
22 mitigated with BW+PA6 blends and the formation of fully deoxygenated compounds was almost  
23 totally suppressed, suggesting that the strong catalyst acid sites were poisoned. Caprolactam was  
24 by far the main product of PA6 degradation found in the bioliquids, but the N-containing by-  
25 products were different depending on the absence or presence of HZSM-5 catalyst. In particular,  
26 the formation of 5-cyano-1-pentene in a fairly large proportion was only observed in the presence  
27 of the catalyst.

28 **Keywords:** Biomass pyrolysis; polyamide pyrolysis; co-pyrolysis; Bio-oils; Catalytic upgrading.

31 1. Introduction

32       Plastics have assumed a crucial role in modern societies. Since the 1950s, the production and  
33 consumption of plastics has grown exponentially due to their multiple properties, such as  
34 versatility, durability, mechanical and chemical inertness, lightness, low cost etc. In 2019, the  
35 global plastic production reached 370 million tons[1]. Plastic materials can be employed in many  
36 sectors such as packaging, building and construction, automotive, electrical and electronics. Thus,  
37 it is expected that a significant part of generated plastic will end in municipal solid waste (MSW)  
38 to be disposed of with other waste materials or incinerated.

39       According to a report on solid waste management published in 2018[2], the world waste  
40 production is expected to increase to 3.4 billion tons by 2050, while the plastic fraction present in  
41 MSW was estimated between 6 and 13 wt.% in 2016, depending on the countries considered.  
42 Indeed, Areeprasert et al.[3] assembled data about the plastics present in MSW from different  
43 countries and the values fluctuated between 3 and 27%. Similarly, Patrício Silva and co-workers[4]  
44 reported plastic concentration between 2 and 20% for different countries. Additionally, these  
45 authors related the impact of the COVID-19 pandemic on the generation of waste plastics, due to  
46 the massive use of personal protective equipment (PPE), achieving a contribution of 3.5% of PPE  
47 in the plastic share of MSW that was sent to various landfill sites around the world in 2020.

48       The European Union fixed the targets of recycling at least 55% of municipal waste by 2025  
49 and 65% by 2035[5]. However, recycling the plastics present in this waste is difficult due to sample  
50 contamination and to the presence of blends of different polymers. In addition, recycling plastic  
51 materials is economically unprofitable due to their low production and processing costs[6].  
52 Therefore, thermal conversion processes such as gasification, incineration and pyrolysis, are  
53 promising alternatives to deal with this complex mixture of solid wastes.

54       Pyrolysis is an interesting process because it can process different types of feedstocks and  
55 allows converting their organic fractions into bio-oils, which can then be integrated into  
56 conventional refinery processes (fluid catalytic cracking or hydroprocessing) to produce fuels, or  
57 be used as a source of high-value products[7,8]. Several studies[9–13] and the recent review by  
58 Ansari et al.[8] reported the beneficial effects of processing plastics and biomass together.  
59 However, the co-pyrolysis of plastic and biomass can be affected by different parameters such as

60 the biomass and plastic types, the biomass to plastic ratio, the process parameters (e.g. temperature,  
61 residence time, heating rate...) and the reactor configuration[14].

62 Table 1 brings together some recent studies devoted to co-pyrolysis of biomass and plastics.

63

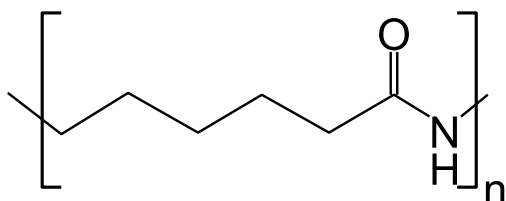
64 Table 1 - Summary of recent publications on co-pyrolysis of biomass and plastics

Reference	Catalyst	Biomass	Catalyst/biomass ratio	Plastic	Plastic/biomass ratio	Conditions
Yu, 2021[15]	HZSM-5	walnut shell	1:8; 1:4; 1:2; 1:1	LDPE	1:1	450 – 850°C
He et al., 2021[12]	HZSM-5	corn stalk	1:1	HDPE	0:1; 4:1; 3:1; 2:1; 1:1; 2:1; 3:1; 4:1; 1:0	550 – 800°C
Qian et al., 2021[16]	Hierarchical ZSM-5	Douglas fir	0.75:1	LDPE	0; 0.15; 0.5; 0.85; 1	429 - 571°C
Dyer, Nahil, and Williams, 2021[17]	ZSM-5	waste wood pellets	2:1	HDPE, LDPE, PP, PS and PET	1:1 and 1:9; 1:4 (only for HDPE and PS)	500°C catalytic bed and temperature ramp of 10°C/min to 500°C
Likun, Zhang, and Fan, 2021[18]	USY and ZSM-5	torrefied bagasse	1:1	HDPE, PS, EVA and PP	1:9; 3:7; 1:1; 7:3	600°C
Praveen Kumar and Srinivas, 2020[9]	Spent FCC catalyst	groundnut shell	1:10	PP and PS	1:2; 1:1; 2:1	510°C
Lin et al., 2020[19]	HZSM-5	corn stover	1:1	HDPE	1:1	550°C
Razzaq et al., 2019[20]	(Fe, Ni, Co, Zn) ZSM-5	wet straw	2:1	PS	1:1	500 - 650°C
Y.-M. Kim et al., 2017[21]	HZSM-5 and Al-MCM-41	torrefied yellow poplar	10:1	HDPE	1:1	600°C
B.-S. Kim et al., 2016[22]	ZSM-5 and HY	cellulose	10:1	PP and LLDPE	1:1	500 and 600°C

65

66 The plastics most frequently studied recently were polyolefins, such as PE and PP, with plastic  
67 concentrations around 50 wt.% and the catalysts employed were essentially zeolites, particularly  
68 ZSM-5. Thus, co-pyrolysis with these main plastics has been exhaustively studied and its impacts  
69 on the pyrolysis process has already been well investigated. As general trends, an increase in the  
70 production of liquid aromatics and a decrease in the formation of light aromatics and chars were  
71 identified.

72 Studies involving plastics that contain heteroatoms, such as N atoms in polyamides, are scarce.  
73 Polyamide-6 (PA6) is a whitish semi-crystalline thermoplastic polymer; its structure is depicted in  
74 Figure 1. It has a wide range of applications due to its properties of high strength, rigidity, chemical  
75 resistance and simple processing. Thus, PA6 is used in the automotive and construction industries,  
76 in electrical and electronic materials, in fibers applied for clothing and, more recently, in the  
77 confection of personal protective equipment (PPE), such as disposable surgical masks[23]. As a  
78 consequence of the COVID-19 pandemic, the concentration of this plastic in MSW has  
79 significantly increased.



80

81 Figure 1 – Structure of polyamide-6

82

83 In this work, the co-pyrolysis beech wood (BW) chips, as lignocellulosic biomass, and PA6  
84 was studied and coupled with catalytic upgrading of the pyrolysis vapors using a HZSM-5 catalyst.  
85 For this purpose, the pyrolysis products (gases, liquids and solids) were characterized in depth  
86 using various analytical techniques, specifically optimized for this type of samples. This study  
87 aims at assessing the role of the catalyst on the products composition after catalytic treatment of  
88 the pyrolysis vapors and the effect of PA6 on the catalytic activity, by comparing experiments  
89 carried out in the absence or in the presence of the catalyst, using pure BW or a blend of BW + 20  
90 wt.% PA6.

91

92 2. Experimental section

93 2.1. Feedstocks

94 The lignocellulosic biomass used consists of beech wood chips supplied by J. Rettenmaier &  
95 Söhne; they were sieved to obtain particle sizes between 0.75 and 1.7 mm. Polyamide-6 (BASF -  
96 Ultramid® B) was supplied as pellets, which were crushed and sieved before use to obtain particle  
97 sizes in the same range as the wood chips. BW chips were mechanically mixed with 5, 10 and 20  
98 wt.% of PA6 (on dry basis). All feedstock samples were dried in an oven at 110°C for 1h before  
99 each pyrolysis experiment and stored in airtight flasks.

100 2.2. Catalyst

101 Zeolite HZSM-5 with a molar Si/Al ratio of 40 was supplied by Céramiques Techniques  
102 Industrielles (CTI) Salindres, France. The catalyst characterization has been described  
103 previously[24] and its main properties are summarized in Table 2.

104 Table 2 - Properties of HZSM-5 catalyst

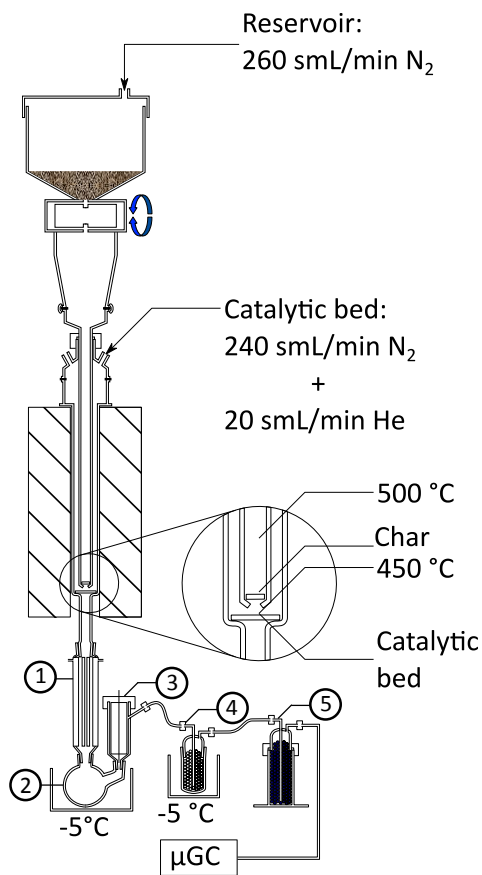
Property	Value
Particle size ( $\mu\text{m}$ )	100-300
Water content <sup>a</sup> (% wt.)	3.9
Si/Al atomic ratio <sup>b</sup> (SAR)	40.5
Total SSA <sup>c</sup> ( $\text{m}^2\text{g}^{-1}$ )	423
Microporous surface ( $\text{m}^2\text{g}^{-1}$ )	363
External surface ( $\text{m}^2\text{g}^{-1}$ )	60
Average pore diameter <sup>d</sup> (nm)	0.55
Total pore volume ( $\text{cm}^3\text{g}^{-1}$ )	0.18
Brønsted acid sites <sup>e</sup> ( $\mu\text{mol/g}$ )	127
Lewis acid sites <sup>e</sup> ( $\mu\text{mol/g}$ )	45

105 <sup>a</sup> measured by TGA; <sup>b</sup> measured by ICP; <sup>c</sup> BET method; <sup>d</sup> from International Zeolite Association  
106 database; <sup>e</sup> measured by FT-IR of pyridine adsorbed at 150°C.

107 Pyrolysis set-up

108 Co-pyrolysis of beech wood and PA6 was carried-out in a lab-scale pyrolytic bench already  
109 described [25], with a few modifications to adapt the system to the mixed wood/plastic feedstocks  
110 (Figure 2). The jacketed reactor has an internal zone where the thermal pyrolysis is carried out and  
111 a bed of catalyst can be placed (or not) just below to treat the vapors which come out of the  
112 pyrolysis zone. The BW chips or BW+PA6 blends were previously dried at 110°C for 1.5 h before  
113 being placed in the gas-tight hopper and kept under N<sub>2</sub> atmosphere.

114 Unlike the previous description [25], the new inner reactor (pyrolysis zone) was a straight  
115 quartz tube, in which the solid chips were fed semi-continuously from the top for 1 h, by small  
116 increments of  $\approx 0.045$  g every 10 s, and fell down by gravity onto a quartz porous frit at the bottom  
117 of this section, where the chars and solid residues were retained. The total mass of solid chips fed  
118 in the reactor was  $\approx 16$  g in 1 h of experiment. The temperature in the pyrolysis zone was 450-  
119 500°C along the tube and 480°C on the porous frit where the wood chips were stopped. The  
120 pyrolysis vapors (formed by thermal pyrolysis) were entrained downstream by a nitrogen flow of  
121 260 smL/min and passed through the catalyst bed (in catalytic experiments) placed just below the  
122 pyrolysis zone on a second quartz frit. The temperature of the catalyst bed was  $453 \pm 2^\circ\text{C}$ . In this  
123 external part of the reactor, an additional gas flow composed of 240 smL/min N<sub>2</sub> and 20 smL/min  
124 He (internal standard) was added to prevent retro-diffusion of the vapors and to adjust the total gas  
125 flow rate. The residence time of the vapors in the pyrolysis zone was estimated at 41 s, while the  
126 contact time with the catalyst (when present) was around 2 s. The pressure in the reactor was  
127 continuously monitored by a pressure sensor connected to a safety device which cuts off the  
128 experiment automatically if the pressure exceeds 1.3 bars. The pressure measured during the  
129 experiments was 1.1-1.15 bar.



130

131 Figure 2 - Pyrolysis setup scheme

132 The vapors were condensed downstream the reactor and collected in a series of traps including  
 133 a condenser (1) and a round bottom flask (2) both cooled at  $-5^{\circ}\text{C}$ , an electrostatic precipitator (3),  
 134 a trap filled with glass beads at  $-5^{\circ}\text{C}$  (4) and a trap at ambient temperature filled with silica gel  
 135 beads (5), that prevented any condensable compound from being introduced in the micro-GC for  
 136 online gas phase analysis. The total mass of bio-oils formed in the experiments was assessed by  
 137 mass difference, by weighing the different glassware parts before and after the experiments.

138 Prior to starting the reaction, the reactor (empty in thermal experiments, or loaded with 2 g of  
 139 catalyst in *ex-situ* catalytic experiments) was heated to  $500^{\circ}\text{C}$  under a  $\text{N}_2$  flow for 2 h to ensure  
 140 fully stabilized temperatures in the whole system (reactor and cold traps) and to desorb the water  
 141 adsorbed on the catalyst.

142

143 2.3. Products recovery

144 Non-condensable products (hereinafter called “gas phase”) were analyzed and quantified  
145 online using a micro-GC.

146 The fractions called “aqueous phase” and “organic phase” were recovered directly in the round  
147 bottom flask and simply separated by centrifugation; thus, they constituted the most representative  
148 share of the bio-oil produced in the process. Other fractions of bio-oils were also deposited in the  
149 downstream traps and remained stuck on the glassware parts. In order to obtain a detailed mass  
150 balance, these fractions were recovered by washing the glassware with methanol, followed by  
151 evaporation of the methanol at 50°C under a pressure of 400 mbar, yielding the “recovered organic  
152 phase”. However, the evaporation step was found to modify the composition of this bio-oil fraction  
153 due to simultaneous evaporation of volatile components. In addition, <sup>13</sup>C-NMR analysis showed  
154 the presence of residual methanol in this fraction. Therefore, it was decided not to mix the  
155 “recovered organic phase” with the native “organic phase”. Finally, a part of the bio-oil could not  
156 be recovered because it was adsorbed on the silicagel beads or lost during the different steps of  
157 recovering the other fractions. This fraction was called “organic not recovered” and was quantified  
158 by weighing the glassware parts before and after experiment.

159 The chars were recovered from the first quartz frit, weighed and are hereinafter called “solid  
160 phase”.

#### 161 2.4. Product characterization

162 Gaseous products were analyzed online using a micro gas chromatograph Inficon 3000 (SRA  
163 instruments) equipped with three analytical modules and TCD detectors, calibrated with  
164 appropriate compound mixtures. A MolSieve column equipped with a Plot U pre-column was used  
165 to analyze He, H<sub>2</sub> and CO; a Plot U column was used to analyze CO<sub>2</sub>, C<sub>2</sub>H<sub>4</sub> and C<sub>2</sub>H<sub>6</sub>; an alumina  
166 column was used to analyze the remaining hydrocarbons (C<sub>3</sub>-C<sub>5</sub>). The duration of each analysis  
167 was 6 minutes and the analyses followed each other for 90 minutes. Helium was used as internal  
168 standard to account for the variations of total gas flow rates at the reactor inlet and outlet.

169 Elemental compositions (CHNS) were obtained with a Flash2000 (Thermo Scientific)  
170 equipment. For each analysis, a known mass of sample (1-3 mg) was placed in a tin crucible and  
171 the experiment was repeated three times to determine the measurement uncertainty.

172 The HHV was calculated from the elemental analysis using the equation proposed by  
173 Channiwala and Parikh [26].

$$174 \quad \text{HHV} = 0.3491[\text{C}] + 1.1783[\text{H}] - 0.1034[\text{O}] - 0.0151[\text{N}]$$

175 In this equation the HHV is expressed in MJ/kg and [C], [H], [N] and [O] in mass percentages  
176 on dry basis. This equation is valid for the range of values: C: 0.00 – 92.25 %; H: 0.43 – 25.15%;  
177 O: 0.00 – 50.00%; N: 0.00 – 5.60%.

178 The water content of bio-oils was determined by Karl-Fischer (KF) titration using a Metrohm  
179 Titrand 852 analyzer. The samples were diluted in THF at a concentration of 10 wt.% and the  
180 volumetric method was employed. To avoid side reactions of aldehydes and ketones with  
181 traditional KF reagents, which produce water, specific reagents for samples containing these  
182 organic compounds were chosen: Karl Fischer ROTI hydroquant C5K (5 mg of water/mL of  
183 solution) and Karl Fischer ROTI hydroquant working medium K. The calibration was carried out  
184 using a solution of 10 wt.% of H<sub>2</sub>O in THF.

185 Molar mass distributions were obtained by gel permeation chromatography (GPC) using an  
186 Agilent equipment (1200 series) equipped with two PL gel columns with different pore sizes (500  
187 and 50 Å) using THF as the mobile phase (1 mL/min). Two detectors were used, a refractive index  
188 detector (RID) and diode-array detector (DAD), collecting data each 0.4 s in the range of 200-450  
189 nm with a resolution of 2 nm. The samples were prepared with concentration of 1 wt.% in THF  
190 and filtered before analysis (PTFE – 0.45µm). The measurements were carried out at 35°C and the  
191 calibration was performed using hydrocarbons standards (molecular weight between 86 and 1000  
192 g/mol).

193 <sup>13</sup>C nuclear magnetic resonance (<sup>13</sup>C-NMR) spectra were recorded using a Bruker AVANCE  
194 400 MHz spectrometer and the spectra were analyzed with the TopSpin 3.0 software. The analyses  
195 were carried out at room temperature with an accumulation of 4500 scans. Trioxane was used as  
196 internal standard, diluted in DMSO-D<sub>6</sub> in a coaxial tube configuration that prevented the contact  
197 of the solvent with the bio-oil samples.

198 Gas chromatography coupled with a mass spectrometer was performed with a GCMS-QP2010  
199 SE apparatus (Shimadzu) equipped with a Zebron ZB Wax-Plus column (length 60 m, internal  
200 diameter 0.25 mm, film thickness 0.25 µm). The samples were diluted in methanol (20 wt.% for

201 organic phase and 30 wt.% for aqueous phase) and filtered before the analysis (Cellulose acetate  
202 – 0.45 $\mu$ m). The oven temperature program started at 70 °C (held for 10 min), then was heated at a  
203 rate of 5°C/min up to 150 °C. At this point the heating rate changed to 3°C/min up to 250 °C (held  
204 for 15 min).

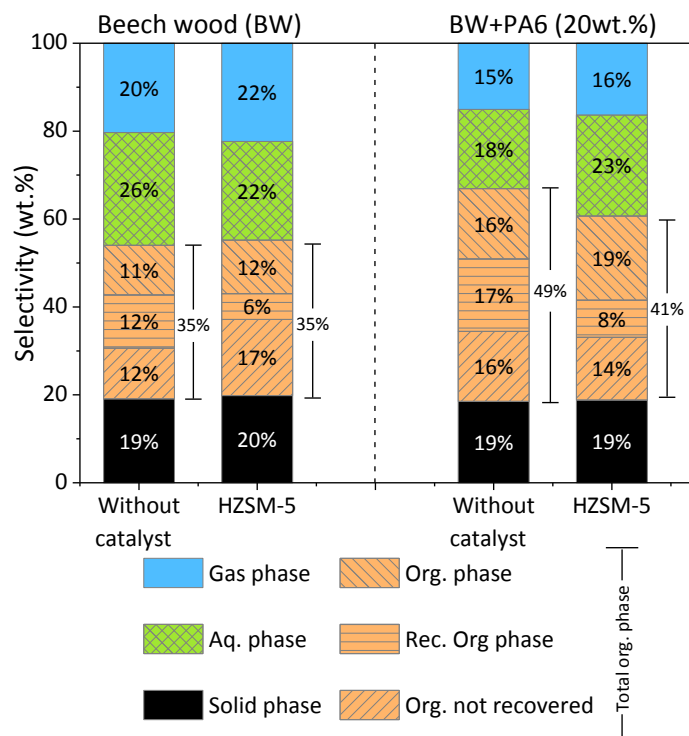
205 Two-dimensional gas chromatography coupled with mass spectrometry (GCxGC-MS) was  
206 carried out with an Agilent GC 6890N apparatus. The first separation was performed by a polar  
207 column VF-1701 MS (I.D 0.25 mm; film thickness 0.25  $\mu$ m; length 30 m) followed by a second  
208 apolar column DB1 (I.D 0.25 mm; film thickness 0.25 $\mu$ m; length 1.5m) for the second dimension  
209 of separation. The modulation was performed by a cryogenic modulator (Zoex Corporation USA)  
210 each 12s. The compounds were identified by the coupled MS detector (5975B). The use of a first  
211 polar column followed by a less polar column favored the separation of oxygen and nitrogen-  
212 containing compounds, widely present in bio-oils[27]. The temperature program was set as  
213 follows: first column from at 50°C to 300 °C with a ramp of 1.75 °C/min, then to 320°C with a  
214 ramp of 1.8 °C/min. The second column went from 50 °C to 320°C at 1.8 °C/min. The samples  
215 concentration was the same as described for GC-MS analyses.

216 The spent catalyst (recovered after reaction) was analyzed by thermogravimetric analysis  
217 (TGA) under air (40 mL/min) using a TGA/DSC-1- Star<sup>e</sup> system (Mettler Toledo) equipped with  
218 a gas controller GC200. The temperature was initially held at 25°C for 5 minutes, then increased  
219 up to 900°C with a heating rate of 10°C/min.

## 220 3. Results and discussion

### 221 3.1. Characterization of pyrolysis and co-pyrolysis products

222 To assess the effect of ex-situ catalytic treatment of pyrolysis vapors, the results obtained with  
223 and without catalyst (HZSM-5) have been compared for experiments with pure beech wood (BW)  
224 or a blend of BW + 20 wt. % PA6. The mass balance was close to 100 % in all experiments (98-  
225 103 %) and liquid products were the main fraction obtained, representing 57-67 wt.% of the total  
226 mass of products. Figure 3 displays the selectivity for solid, liquid and gas products, calculated as  
227 the mass of a given fraction over the total mass of products. In the absence of a catalyst, the mass  
228 of solid products corresponded to those collected on the first frit glass at the outlet of the pyrolysis  
229 zone, while in the presence of the catalyst it also included the mass of coke deposited on the spent  
230 catalyst, which was also quantified separately.

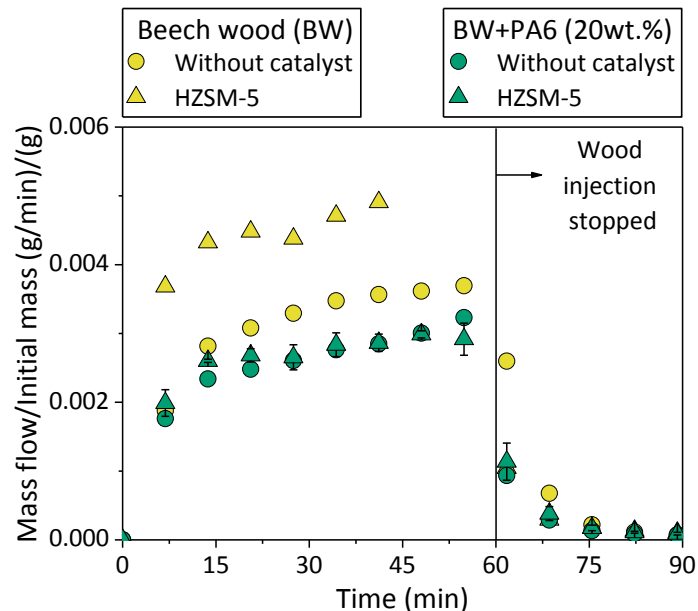


231

232 Figure 3 - Product selectivity in experiments with pure BW and BW+PA6 (20%) blends

233 For both feedstocks, the total mass of liquid products (aqueous + organic phases) decreased in  
 234 the presence of HZSM-5, while the mass of gaseous products increased slightly. The selectivity  
 235 towards the organic phase was higher with BW + PA6 than with pure BW, and with BW + PA6  
 236 the selectivity for the organic phase was higher in thermal than in catalytic pyrolysis.

237 Regarding the gas products, the increase in the formation of non-condensable gases in the  
 238 presence of HZSM-5 is due to its strong acid sites that promote the cracking of pyrolysis vapors  
 239 into small compounds [28,29]. This effect, however, was marginal when BW + PA6 was used.  
 240 Figure 4 shows the total mass of gases produced, normalized by the mass of feedstock. The  
 241 experiment with catalyst and 20% of PA6 (▲) was repeated 3 times and the error bar is displayed  
 242 on the figure.



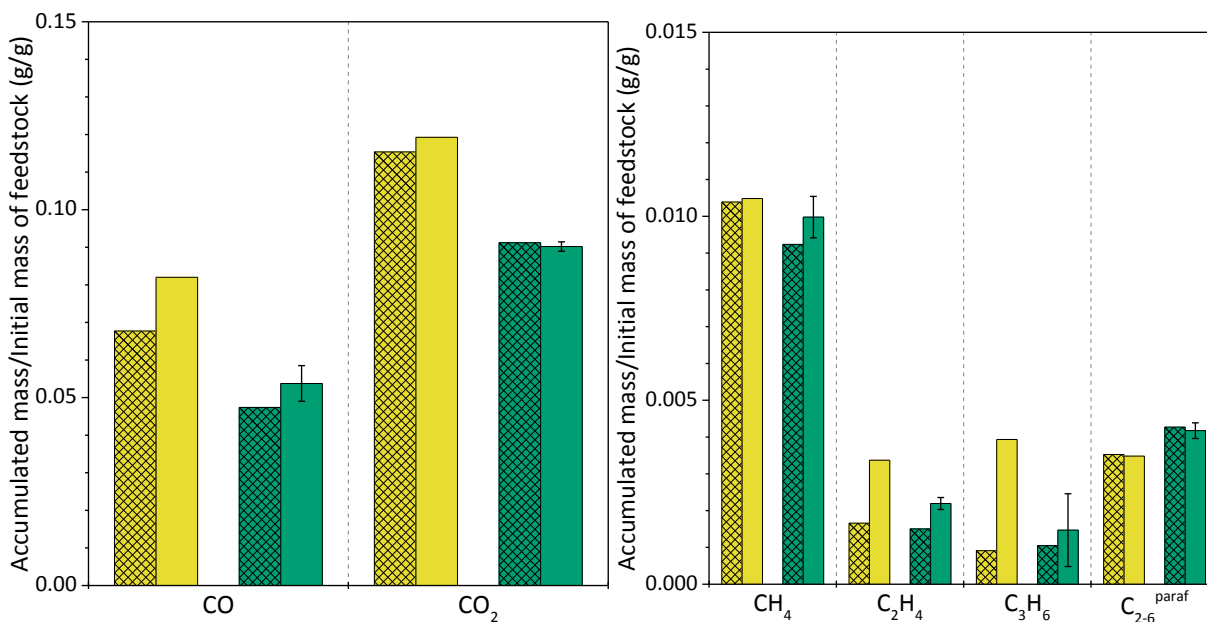
243

244 Figure 4 - Total mass flow of gaseous products normalized by the initial mass of feedstock

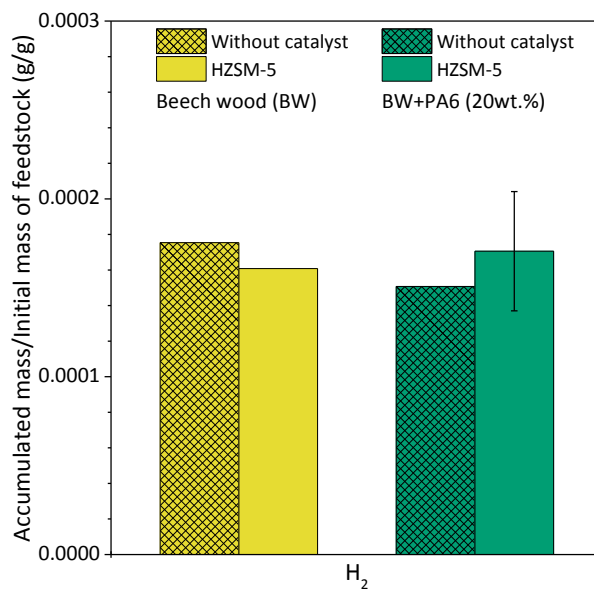
245 The increase in gas production in the presence of HZSM-5 was significant in experiments with  
 246 BW. However, this effect was marginal when PA6 was added to BW: although in the first 20 min  
 247 there were slightly more gases produced in the presence of HZSM-5 (▲), afterwards no more  
 248 difference was noticeable compared to experiments without a catalyst (●) and the trend ended up  
 249 being reversed for the last data point. This suggests a catalyst deactivation in the presence of PA6,  
 250 which seems likely related to the adsorption of N-containing compounds on acid sites than to coke  
 251 deposition, given that the two data sets were close at the reaction onset. The decomposition of PA6  
 252 resulted mainly in caprolactam, as will be discussed later, but it can also generate compounds such  
 253 as pyrroles that may remain adsorbed even at high temperatures.

254 Figure 5 shows the detailed product distribution in the gas phase.

255



256



257

Figure 5 - Cumulative mass of NCG normalized by the initial mass of feedstock

258

259

260

261

262

263

264

Whatever the feedstock used, CO and CO<sub>2</sub> were the main products in all experiments, representing almost 90% of the total mass of gaseous products. In the presence of HZSM-5, the CO production increased slightly, particularly when using BW, whereas the CO<sub>2</sub> production did not change significantly. Indeed, in literature[30–33], the strong Brønsted acid sites present in HZSM-5 have been reported as being more efficient to remove oxygen from biomass through decarbonylation of carbohydrate-derived compounds rather than through decarboxylation reactions. Methane was also the main light hydrocarbon produced whatever the conditions used,

265 while the yields of light olefins (ethylene and propylene) increased strongly in the presence of  
 266 HZSM-5 when pure BW was used, but less significantly with BW + PA6. Finally, the hydrogen  
 267 production, which represented less than 0.1 wt.%, was similar in all experiments (the differences  
 268 observed were within the margin of error).

269 The water content, the ultimate analysis and the HHV of the organic and aqueous phases are  
 270 shown in Table 3.

271 Table 3 - Water content, ultimate analysis and higher heating value of organic and aqueous  
 272 phases

	%H <sub>2</sub> O	Elemental analysis (wt.% on dry basis)				HHV (MJ/kg)
		C	H	N	O*	
<b>Organic phase</b>						
Beech wood						
no catalyst	18.7±1.0	65.4±1.0	6.0±0.4	0.6±0.1	28.0±1.5	27.0±1.0
HZSM-5	11.9±1.8	70.6±1.2	6.4±0.6	0.5±0.6	22.4±0.6	30.0±0.2
BW + 20% PA6						
no catalyst	21.2±0.3	66.1±1.0	7.2±0.2	5.1±0.4	21.6±0.7	29.3±0.6
HZSM-5	13.8±1.4	71.6±2.4	7.5±0.5	6.1±0.4	14.8±2.2	32.2±0.7
<b>Aqueous phase</b>						
Beech wood						
no catalyst	48.3±1.2	52.1±0.4	6.2±3.0	1.2±0.6	40.4±2.6	21.3±3.8
HZSM-5	78.9±1.3	61.3±1.6	3.9±3.2	2.1±1.3	32.7±2.2	23.5±2.6
BW + 20% PA6						
no catalyst	56.2±0.1	60.7±2.5	6.4±2.8	6.2±0.8	26.7±1.6	25.9±2.7
HZSM-5	65.8±2.3	54.5±1.8	6.2±7.2	8.7±1.8	30.6±5.3	23.1±8.9

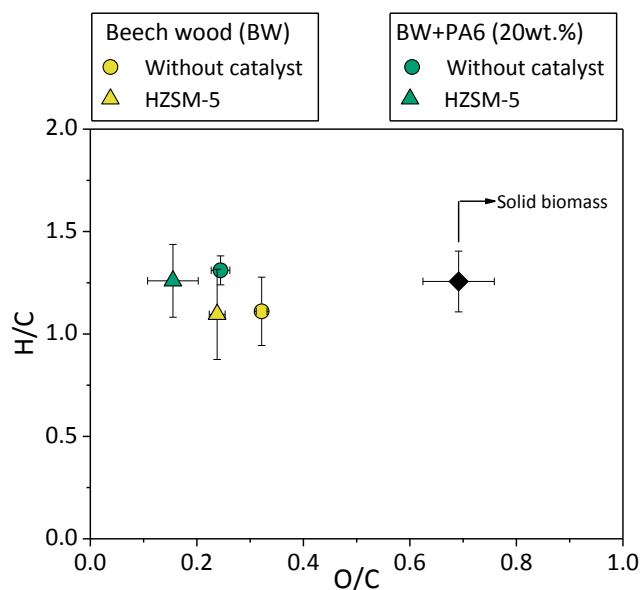
273 \*by difference

274 The effect of the catalyst was obvious considering the water content of the organic and aqueous  
 275 phases: the organic phase obtained after *ex situ* catalytic treatment contained about half as much  
 276 water, whereas the aqueous phase contained more water. Besides the decarbonylation and  
 277 decarboxylation reactions mentioned previously, the oxygen from biomass-derived oligomers can  
 278 be removed through dehydration of OH groups, which results in water formation [34–36]. Using  
 279 BW, the total yield of water (sum of water content in organic and aqueous phases) changed from  
 280 19 without a catalyst to 21.5 % in the presence of HZSM-5. Changing the concentration of water  
 281 in the organic and aqueous phases also modifies their polarity and consequently the products

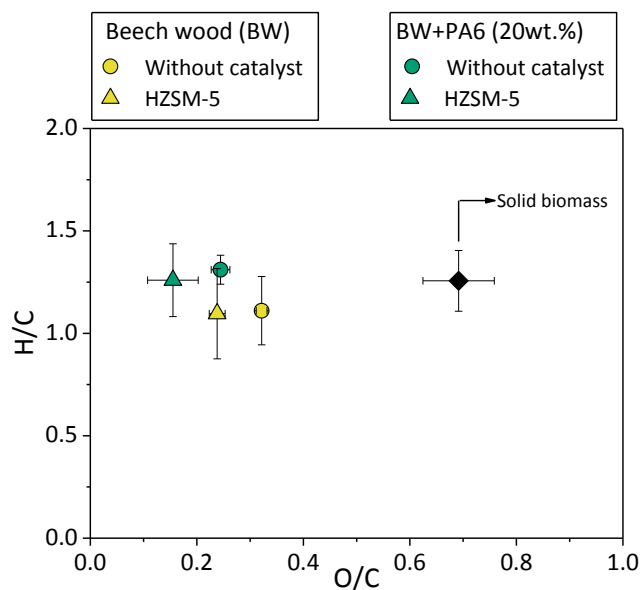
282 distribution between the two phases, depending on their more or less polar nature. Polar  
283 compounds such as acids and sugars will tend to remain in the aqueous phase during the phase  
284 separation process. Although the effect of the catalyst was still very clear with BW + PA6, it was  
285 less important, confirming a partial catalyst deactivation related to PA6.

286 The nitrogen content in both organic and aqueous phases was much higher when BW + PA6  
287 was used, and also higher in the presence of the zeolite, which suggests that the catalyst also  
288 promoted the depolymerization of PA6, leading to small N-compounds that are condensed in the  
289 liquid fractions.

290 The Van Krevelen diagram obtained for the organic phases is shown in



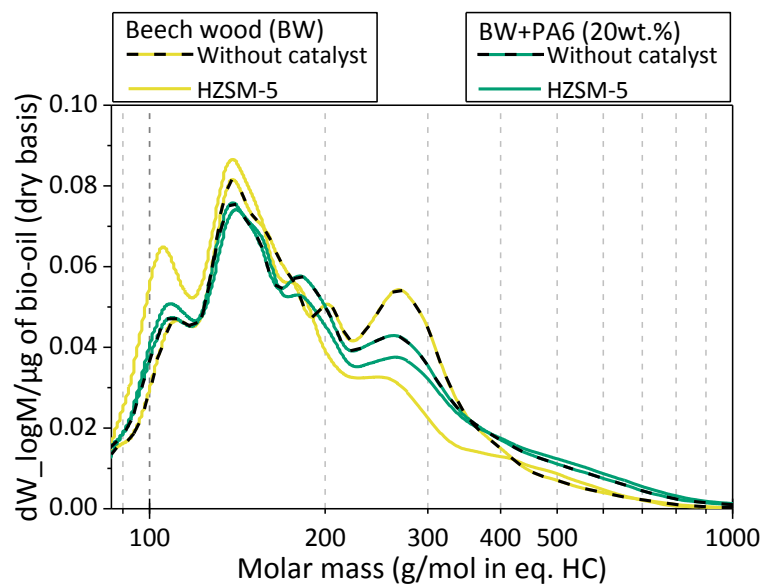
291  
292 Figure 6. With both feedstocks, the effect of HZSM-5 on the deoxygenation of bio-oils was  
293 evidenced by the shift to the left of O/C ratios compared to un-catalyzed experiments. The H/C  
294 ratio remained close to that of the initial biomass. A similar figure with N/C ratios as a function of  
295 H/C ratios can be found in the supplementary information (Fig. S1).



296

297 Figure 6 - Van Krevelen diagram of organic phases (on dry basis).

298 The molar mass distribution of organic fractions is presented in Figure 7. The refractive index  
 299 detector (RID) signal ( $dw_{\log M}$ ) was normalized by the mass of dry bio-oil used in each analysis.  
 300 For experiments with pure BW, the catalyst caused the peak at  $\approx 270$  g/mol (in eq. HC) to decrease  
 301 and the peak at  $\approx 100$  g/mol (in eq. HC) to increase, while the average molar mass decreased from  
 302 210 to 191 g/mol (in HC equivalent). This behavior can be associated to the promotion of biomass  
 303 depolymerization in the presence of the catalyst. Conversely, when plastic was added to the  
 304 feedstock, this difference was less pronounced and the average molar mass did not change in the  
 305 presence of the catalyst (219 g/mol in HC eq.).



306

307 Figure 7 – GPC molar mass distribution of organic phases

308 <sup>13</sup>C-NMR (Figure 8) was used to identify the different functional groups that can be found in  
 309 the bio-oils. It allows a global analysis of all bio-oils components, independently of their solubility  
 310 in solvents and without any limitation of molar mass range or volatility/thermal stability. The  
 311 functional groups and their respective chemical shifts were reported in previous  
 312 publications[24,25].

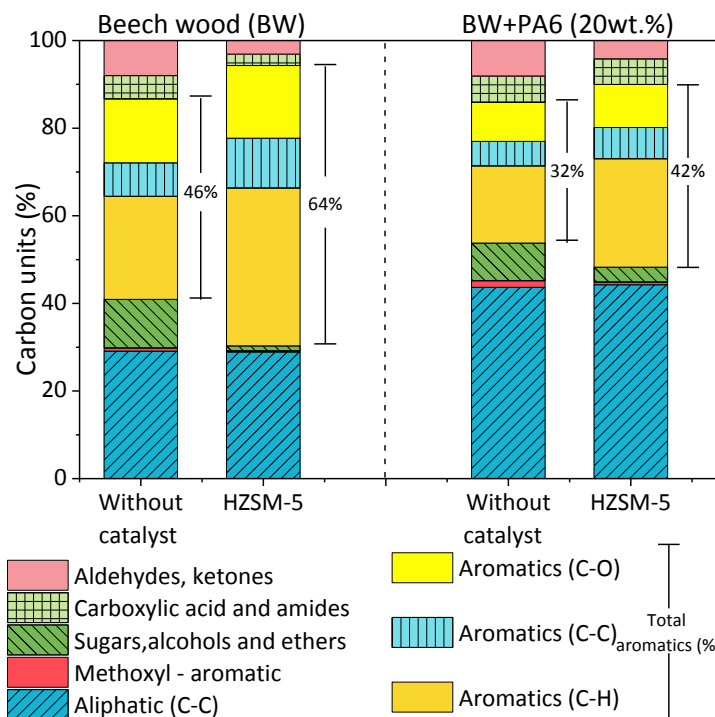


Figure 8 - <sup>13</sup>C-NMR functional group distribution in the organic phases

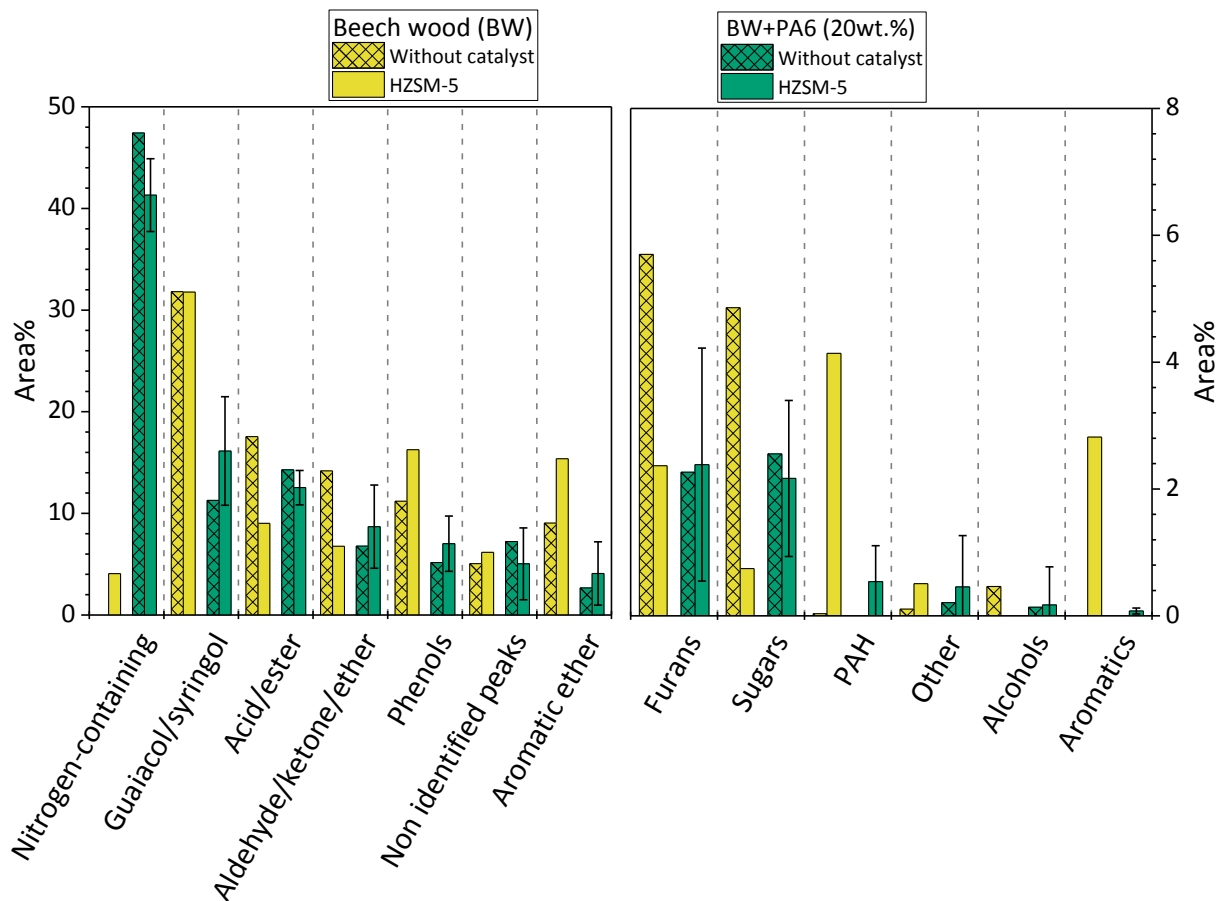
313

314

315 The presence of the catalyst resulted in an increase in the production of aromatics (from 46 to  
 316 64% using BW only); when using BW + PA6, however, this increase was less pronounced.  
 317 Similarly, the decrease in sugars, alcohols and ethers production was less significant when PA6  
 318 was present in the feedstock. This corroborates the hypothesis of a partial deactivation of acid sites,  
 319 which are responsible for the reactions of cracking, aromatization and deoxygenation [16,37–39].  
 320 In addition, a significant increase in aliphatic C-C units was observed in co-pyrolysis experiments,  
 321 which could be attributed to the production of compounds originating from the degradation of  
 322 PA6.

323 GC-MS analyses provided a more detailed insight on the composition of bio-oils, in terms of  
 324 compounds identification. Due to the large number of compounds present in the bio-oils, the  
 325 calibration of each compound was not possible and the analysis was hence not quantitative, but  
 326 the peak areas of similar compounds can be compared. The compounds that can be analyzed using  
 327 GC-MS are also limited to molecules that can be vaporized in the injector without decomposition  
 328 (which probably excludes some sugars) and elute at 250°C (maximum temperature that can be  
 329 applied to the column). The main groups of compounds produced by pyrolysis of beech wood  
 330 identified by GC-MS have been published previously[24,25]. The detailed list of compounds

331 identified individually using their mass fragmentation spectra can be found in the supporting  
 332 information. The characterization of the organic fractions obtained in the present study are  
 333 displayed in Figure 9.

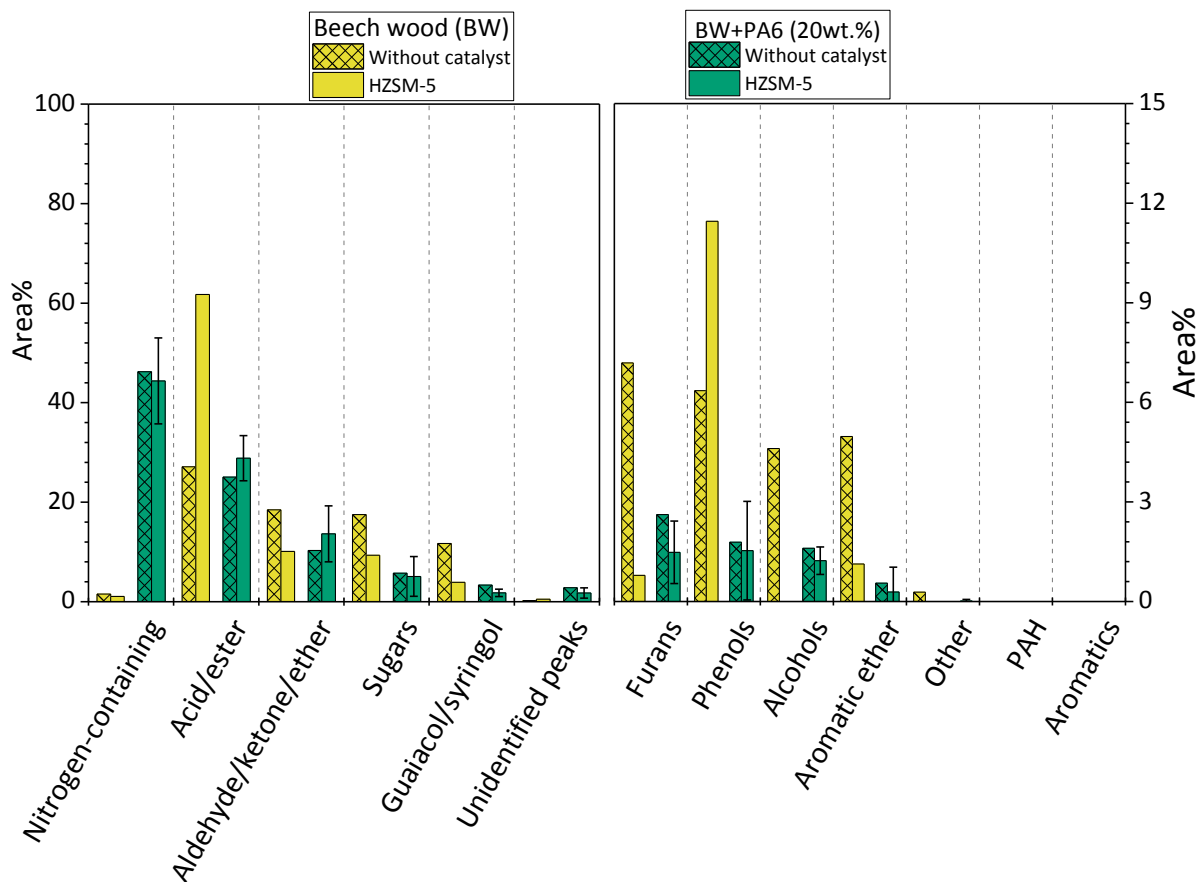


334  
 335 Figure 9 - Relative areas of compounds families identified by GC-MS for the organic phases

336 As observed with  $^{13}\text{C}$ -NMR, GC-MS analyses also showed that the presence of the catalyst  
 337 resulted in an increase in aromatic compounds families such as phenols and aromatic ethers, but  
 338 this increase was less significant for experiments making use of BW + PA6. Furthermore, the  
 339 effect of the catalyst in reducing the amounts of furans and sugars was clearly diminished in the  
 340 presence of PA6, in agreement with the reduced production of CO, CO<sub>2</sub>, confirming a partial  
 341 catalyst deactivation[34,40]. Finally, the formation of aromatic and polyaromatic deoxygenated  
 342 compounds (PAH), which was observed only in the presence of HZSM-5 catalyst, was drastically  
 343 reduced with BW + PA6, suggesting that the catalytic sites responsible for their formation were  
 344 almost totally suppressed.

345

Figure 10 shows the GC-MS analyses of the aqueous phase.



346

347 Figure 10 - Relative areas of compounds families identified by GC-MS for aqueous phase

348 Using pure BW, the HZSM-5 catalyst led to a strong increase in the concentration of acid/ester  
349 and phenol families in the aqueous phase. This trend was strongly mitigated using BW + PA6,  
350 which can also be associated to the catalyst deactivation. Organic acids, especially acetic acid, can  
351 be produced by depolymerization of the three biopolymers constitutive of lignocellulosic biomass  
352 (cellulose, hemicellulose and lignin), but hemicellulose mainly contributes to the formation of  
353 organic acids by cleavage of the acetyl groups linked to the polysaccharide structure [41–44].  
354 These reactions are promoted by acid sites and the poisoning of these sites might impair the  
355 production of such compounds.

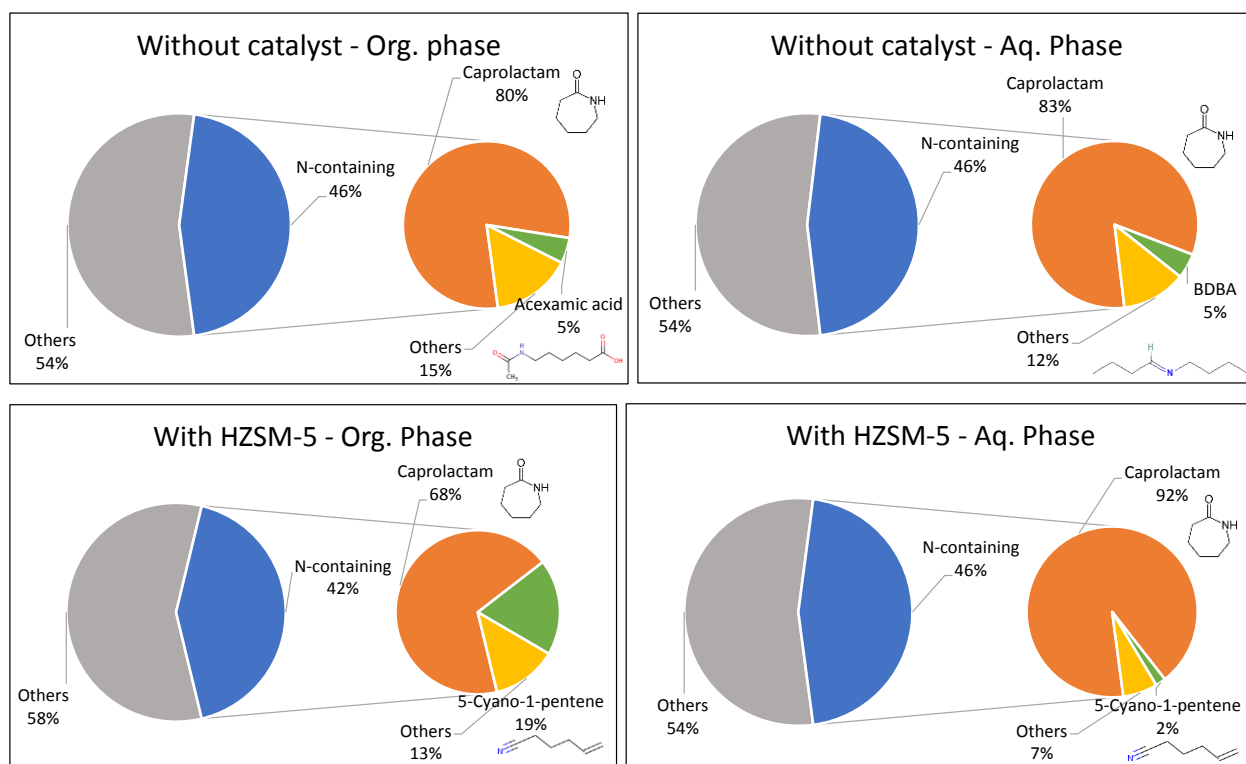
356 GC-MS analyses also provided a specific insight on N-compounds. Bio-oils prepared from  
357 pure beech wood contained small amounts of nitrogen compounds, as shown in Table 3, from the  
358 presence in the wood of proteins involved in biological functions and plants metabolism. The bark

359 of beech trees also contains chlorophyll, of which the four pyrrole rings can decompose into N-  
360 compounds. Three compounds were identified: 1-(2-propenyl)-piperidine (1.92 % of the total peak  
361 area), 5,6-dihydro-5-methyl-uracil (1.46 %) and 3-methylpyridazine (0.53 %).

362 In order to better understand the impact of the catalyst on the degradation PA6, Figure 11  
363 presents the main N-containing products analyzed in the organic and aqueous phases. Over 100  
364 compounds were identified, the complete list of which can be found in the supplementary  
365 information. However most of them are present only in very small amounts.

366

367

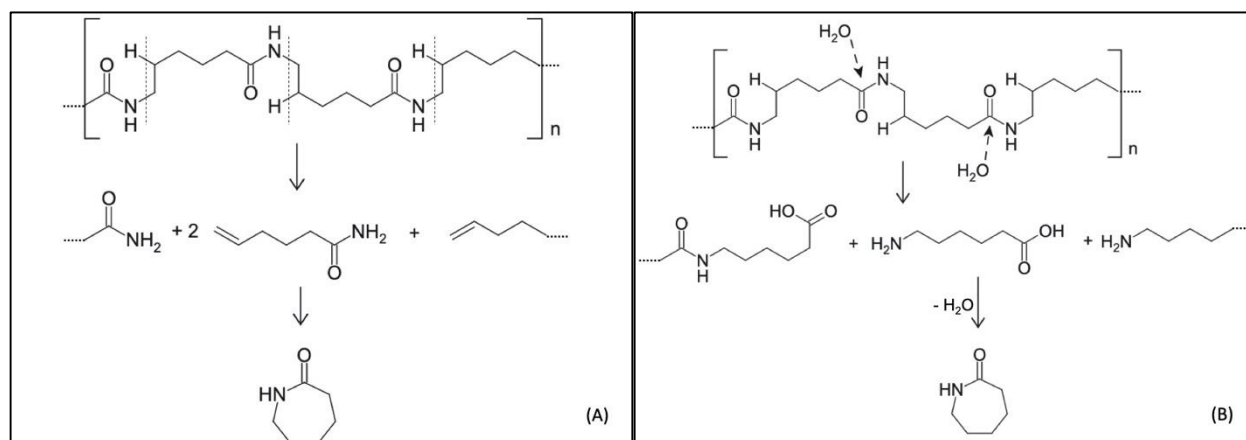


368

369 Figure 11 - N-containing products distribution in organic and aqueous phases obtained by pyrolysis  
370 of BW+PA6 without or with HZSM-5 catalyst

371 In all experiments, caprolactam was by far the main product, in agreement with the literature  
372 [45–49], and it was found in both organic and aqueous phases. This compound can be formed by  
373 two reaction pathways: (i) cleavage of two C-N bonds of the polymeric chain and cis-elimination,  
374 leading to formation of hexene-5-amide, followed by cyclization into caprolactam (Figure 12A),  
375 or (ii) hydrolysis of two amide linkages of PA6, leading to the formation of aminocaproic acid,

376 also followed by cyclization [46,47] (Figure 12B). This pathway could be preferred in the presence  
 377 of BW, the pyrolysis of which produces a lot of water. Bockhorn et al. found that the thermal  
 378 pyrolysis of pure PA6 between 380 and 460°C led to caprolactam being formed with yields >92%  
 379 [47]. This suggests that in co-pyrolysis of PW+PA6 blends, the presence of wood-derived products  
 380 decreased the selectivity of PA6 degradation. The secondary products differed depending on the  
 381 presence or not of the catalyst. Without a catalyst, the secondary products are also formed through  
 382 cleavage of C-N bonds of PA6, but without cyclization, leading to linear compounds such as  
 383 acexamic acid found in the organic phase, and N-butylidene-1-butanamine (BDBA) found in the  
 384 aqueous phase. When *ex situ* catalytic treatment of vapors was applied, 5-cyano-1-pentene was the  
 385 second most abundant product identified in both phases. This linear mono-nitrile can be formed  
 386 by dehydration of caprolactam, catalyzed by Brønsted acid sites [49,50], which clearly exemplifies  
 387 the effect of HZSM-5 catalyst in modifying the composition of bio-oils.



389 Figure 12: Possible reaction pathways for the formation of caprolactam from PA-6.

390

### 391 3.2. Coke deposition on the spent catalyst

392 The catalyst was heavily coked after pyrolysis: the coke content was 13.4 wt.% after pyrolysis of  
 393 BW and 11.8 wt.% after co-pyrolysis of BW+PA6, which suggests that PA6 contributed to  
 394 reducing the catalyst coking. Ultimate analysis of this coke, however, revealed that the N-content  
 395 of this coke was 0.5 wt.% after pyrolysis of BW and 6.1 wt. % after pyrolysis of BW+PA6, a  
 396 twelve-fold increase much greater than could be expected from the initial PA6 concentration in  
 397 the feedstock (20 wt.%). This confirms that N-containing compounds derived from PA6 adsorb on

398 the catalyst more strongly than compounds derived from BW and are probably responsible for the  
399 catalyst deactivation.

400

#### 401 4. Conclusion

402 In this study, the co-pyrolysis of a N-containing plastic, polyamide-6 (PA6) and beech wood  
403 (BW) was investigated in the absence or presence of a HZSM-5 catalyst for *ex-situ* treatment of  
404 the pyrolysis vapors. The catalyst modified the composition of pyrolysis oils and products  
405 distribution in both liquid phases (aqueous and organic). Compared to the pyrolysis of pure BW,  
406 the effect of the catalyst on the composition of pyrolysis oils was less pronounced in the presence  
407 of the plastic, due to a partial catalyst deactivation, which essentially affected its deoxygenation  
408 properties. This deactivation can be assigned to the adsorption of N-containing compounds,  
409 produced by degradation of PA6, on strong acid sites of the zeolite that are responsible for the  
410 formation of deoxygenated compounds. Despite this deactivation, the catalyst remained capable  
411 of promoting the depolymerization of BW and PA6, which led to an increase in the concentration  
412 of N-containing products in the liquid phases, with caprolactam as the main product. The catalyst  
413 also modified the N-containing by-products found in bio-oils, notably the formation of 5-cyano-  
414 1-pentene was observed only in the presence of HZSM-5 catalyst.

415

#### 416 ACKNOWLEDGEMENTS

417 This project has received funding from the European Union's Horizon 2020 research and  
418 innovation programme under grant agreement N° 818120 (Waste2Road ). The authors also  
419 thank Véronique Bounor-Légaré (CNRS and University of Lyon) for providing different samples  
420 of plastics.

421

#### 422 References

423 [1] PlasticsEurope, Plastic - the Facts 2020, Association of plastics Manufacturers, 2020.  
424 [https://www.plasticseurope.org/application/files/3416/2270/7211/Plastics\\_the\\_facts-WEB-](https://www.plasticseurope.org/application/files/3416/2270/7211/Plastics_the_facts-WEB-2020_versionJun21_final.pdf)  
425 [2020\\_versionJun21\\_final.pdf](https://www.plasticseurope.org/application/files/3416/2270/7211/Plastics_the_facts-WEB-2020_versionJun21_final.pdf) (accessed October 22, 2021).

- 426 [2] S. Kaza, L.C. Yao, P. Bhada-Tata, F. Van Woerden, What a Waste 2.0 : A Global Snapshot  
427 of Solid Waste Management to 2050, World Bank, 2018.  
428 <https://openknowledge.worldbank.org/handle/10986/30317>.
- 429 [3] C. Areeprasert, J. Asingsamanunt, S. Srisawat, J. Kaharn, B. Inseemeeesak, P. Phasee, C.  
430 Khaobang, W. Siwakosit, C. Chiemchaisri, Municipal Plastic Waste Composition Study at  
431 Transfer Station of Bangkok and Possibility of its Energy Recovery by Pyrolysis, Energy  
432 Procedia. 107 (2017) 222–226. <https://doi.org/10.1016/j.egypro.2016.12.132>.
- 433 [4] A.L. Patrício Silva, J.C. Prata, A.C. Duarte, D. Barcelò, T. Rocha-Santos, An urgent call to  
434 think globally and act locally on landfill disposable plastics under and after covid-19  
435 pandemic: Pollution prevention and technological (Bio) remediation solutions, Chemical  
436 Engineering Journal. 426 (2021) 131201. <https://doi.org/10.1016/j.cej.2021.131201>.
- 437 [5] C. of the E.U. European Parliament, Directive 2009/28/EC of the European Parliament and  
438 of the Council of 23 April 2009 on the promotion of the use of energy from renewable  
439 sources and amending and subsequently repealing Directives 2001/77/EC and 2003/30/EC,  
440 (2009) 47.
- 441 [6] D. Phakedi, A.U. Ude, P.O. Oladijo, Co-pyrolysis of polymer waste and carbon-based  
442 matter as an alternative for waste management in the developing world, Journal of  
443 Analytical and Applied Pyrolysis. 155 (2021) 105077.  
444 <https://doi.org/10.1016/j.jaap.2021.105077>.
- 445 [7] A. Bridgwater, Fast pyrolysis processes for biomass, Renewable and Sustainable Energy  
446 Reviews. 4 (2000) 1–73. [https://doi.org/10.1016/S1364-0321\(99\)00007-6](https://doi.org/10.1016/S1364-0321(99)00007-6).
- 447 [8] K.B. Ansari, S.Z. Hassan, R. Bhoi, E. Ahmad, Co-pyrolysis of biomass and plastic wastes:  
448 A review on reactants synergy, catalyst impact, process parameter, hydrocarbon fuel  
449 potential, COVID-19, Journal of Environmental Chemical Engineering. 9 (2021) 106436.  
450 <https://doi.org/10.1016/j.jece.2021.106436>.
- 451 [9] K. Praveen Kumar, S. Srinivas, Catalytic Co-pyrolysis of Biomass and Plastics  
452 (Polypropylene and Polystyrene) Using Spent FCC Catalyst, Energy Fuels. 34 (2020) 460–  
453 473. <https://doi.org/10.1021/acs.energyfuels.9b03135>.
- 454 [10] K.R.G. Burra, X. Liu, Z. Wang, J. Li, D. Che, A.K. Gupta, Quantifying the sources of  
455 synergistic effects in co-pyrolysis of pinewood and polystyrene, Applied Energy. 302  
456 (2021) 117562. <https://doi.org/10.1016/j.apenergy.2021.117562>.
- 457 [11] X. Liu, K.R.G. Burra, Z. Wang, J. Li, D. Che, A.K. Gupta, Towards enhanced  
458 understanding of synergistic effects in co-pyrolysis of pinewood and polycarbonate,  
459 Applied Energy. 289 (2021) 116662. <https://doi.org/10.1016/j.apenergy.2021.116662>.
- 460 [12] T. He, S. Zhong, C. Liu, A. Shujaa, B. Zhang, Enhancing hydrocarbon production via ex-  
461 situ catalytic co-pyrolysis of biomass and high-density polyethylene: Study of synergistic  
462 effect and aromatics selectivity, Waste Management. 128 (2021) 189–199.  
463 <https://doi.org/10.1016/j.wasman.2021.04.058>.
- 464 [13] Z. Wang, K.G. Burra, T. Lei, A.K. Gupta, Co-pyrolysis of waste plastic and solid biomass  
465 for synergistic production of biofuels and chemicals-A review, Progress in Energy and  
466 Combustion Science. 84 (2021) 100899. <https://doi.org/10.1016/j.peccs.2020.100899>.
- 467 [14] X. Lin, L. Kong, H. Cai, Q. Zhang, D. Bi, W. Yi, Effects of alkali and alkaline earth metals  
468 on the co-pyrolysis of cellulose and high density polyethylene using TGA and Py-GC/MS,  
469 Fuel Processing Technology. 191 (2019) 71–78.  
470 <https://doi.org/10.1016/j.fuproc.2019.03.015>.

- 471 [15] D. Yu, Composite Pyrolysis of Biomass and Plastic for High-quality Fuel Oil over HZSM-  
472 5, *American Journal of Chemical Engineering*. 9 (2021) 39–46. [https://doi.org/doi:  
473 10.11648/j.ajche.20210902.12](https://doi.org/doi:10.11648/j.ajche.20210902.12).
- 474 [16] M. Qian, H. Lei, E. Villota, Y. Zhao, E. Huo, C. Wang, W. Mateo, R. Zou, Enhanced  
475 production of renewable aromatic hydrocarbons for jet-fuel from softwood biomass and  
476 plastic waste using hierarchical ZSM-5 modified with lignin-assisted re-assembly, *Energy  
477 Conversion and Management*. 236 (2021) 114020.  
478 <https://doi.org/10.1016/j.enconman.2021.114020>.
- 479 [17] A.C. Dyer, M.A. Nahil, P.T. Williams, Catalytic co-pyrolysis of biomass and waste plastics  
480 as a route to upgraded bio-oil, *Journal of the Energy Institute*. 97 (2021) 27–36.  
481 <https://doi.org/10.1016/j.joei.2021.03.022>.
- 482 [18] P. Keliona Wani Likun, H. Zhang, Y. Fan, Improving hydrocarbons production via catalytic  
483 co-pyrolysis of torrefied-biomass with plastics and dual catalytic pyrolysis, *Chinese Journal  
484 of Chemical Engineering*. (2021). <https://doi.org/10.1016/j.cjche.2020.09.074>.
- 485 [19] X. Lin, D. Zhang, X. Ren, Q. Zhang, H. Cai, W. Yi, H. Lei, Catalytic co-pyrolysis of waste  
486 corn stover and high-density polyethylene for hydrocarbon production: The coupling effect  
487 of potassium and HZSM-5 zeolite, *Journal of Analytical and Applied Pyrolysis*. 150 (2020)  
488 104895. <https://doi.org/10.1016/j.jaap.2020.104895>.
- 489 [20] M. Razzaq, M. Zeeshan, S. Qaisar, H. Iftikhar, B. Muneer, Investigating use of metal-  
490 modified HZSM-5 catalyst to upgrade liquid yield in co-pyrolysis of wheat straw and  
491 polystyrene, *Fuel*. 257 (2019) 116119. <https://doi.org/10.1016/j.fuel.2019.116119>.
- 492 [21] Y.-M. Kim, J. Jae, B.-S. Kim, Y. Hong, S.-C. Jung, Y.-K. Park, Catalytic co-pyrolysis of  
493 torrefied yellow poplar and high-density polyethylene using microporous HZSM-5 and  
494 mesoporous Al-MCM-41 catalysts, *Energy Conversion and Management*. 149 (2017) 966–  
495 973. <https://doi.org/10.1016/j.enconman.2017.04.033>.
- 496 [22] B.-S. Kim, Y.-M. Kim, H.W. Lee, J. Jae, D.H. Kim, S.-C. Jung, C. Watanabe, Y.-K. Park,  
497 Catalytic Copyrolysis of Cellulose and Thermoplastics over HZSM-5 and HY, *ACS  
498 Sustainable Chemistry & Engineering*. 4 (2016) 1354–1363.  
499 <https://doi.org/10.1021/acssuschemeng.5b01381>.
- 500 [23] BASF, Ultramid® (PA), (n.d.). [https://plastics-  
501 rubber.basf.com/global/en/performance\\_polymers/products/ultramid.html](https://plastics-rubber.basf.com/global/en/performance_polymers/products/ultramid.html) (accessed  
502 October 25, 2021).
- 503 [24] W. de Rezende Locatel, D. Laurenti, Y. Schuurman, N. Guilhaume, Can Paints and Varnish  
504 Impair the Physicochemical Properties of Wood Pyrolysis Oils?, *Energy Fuels*. 35 (2021)  
505 17739–17754. <https://doi.org/10.1021/acs.energyfuels.1c02568>.
- 506 [25] W. de Rezende Locatel, D. Laurenti, Y. Schuurman, N. Guilhaume, Ex-situ catalytic  
507 upgrading of pyrolysis vapors using mixed metal oxides, *Journal of Analytical and Applied  
508 Pyrolysis*. 158 (2021) 105241. <https://doi.org/10.1016/j.jaap.2021.105241>.
- 509 [26] S.A. Channiwala, P.P. Parikh, A unified correlation for estimating HHV of solid, liquid and  
510 gaseous fuels, *Fuel*. 81 (2002) 1051–1063. [https://doi.org/10.1016/S0016-2361\(01\)00131-4](https://doi.org/10.1016/S0016-2361(01)00131-4).
- 511 [27] B. Omais, M. Courtiade, N. Charon, D. Thiébaud, A. Quignard, M.-C. Hennion,  
512 Investigating comprehensive two-dimensional gas chromatography conditions to optimize  
513 the separation of oxygenated compounds in a direct coal liquefaction middle distillate,  
514 *Journal of Chromatography A*. 1218 (2011) 3233–3240.  
515 <https://doi.org/10.1016/j.chroma.2010.12.049>.

- 516 [28] A.V. Bridgwater, Review of fast pyrolysis of biomass and product upgrading, *Biomass and*  
517 *Bioenergy*. 38 (2012) 68–94. <https://doi.org/10.1016/j.biombioe.2011.01.048>.
- 518 [29] B. Luna-Murillo, M. Pala, A.L. Paioni, M. Baldus, F. Ronse, W. Prins, P.C.A. Bruijninx,  
519 B.M. Weckhuysen, Catalytic Fast Pyrolysis of Biomass: Catalyst Characterization Reveals  
520 the Feed-Dependent Deactivation of a Technical ZSM-5-Based Catalyst, *ACS Sustainable*  
521 *Chemistry & Engineering*. 9 (2021) 291–304.  
522 <https://doi.org/10.1021/acssuschemeng.0c07153>.
- 523 [30] A. Corma, G. Huber, L. Sauvanaud, P. Oconnor, Processing biomass-derived oxygenates in  
524 the oil refinery: Catalytic cracking (FCC) reaction pathways and role of catalyst, *Journal of*  
525 *Catalysis*. 247 (2007) 307–327. <https://doi.org/10.1016/j.jcat.2007.01.023>.
- 526 [31] A.J. Foster, J. Jae, Y.-T. Cheng, G.W. Huber, R.F. Lobo, Optimizing the aromatic yield and  
527 distribution from catalytic fast pyrolysis of biomass over ZSM-5, *Applied Catalysis A:*  
528 *General*. 423–424 (2012) 154–161. <https://doi.org/10.1016/j.apcata.2012.02.030>.
- 529 [32] K. Wang, K.H. Kim, R.C. Brown, Catalytic pyrolysis of individual components of  
530 lignocellulosic biomass, *Green Chemistry*. 16 (2014) 727–735.  
531 <https://doi.org/10.1039/C3GC41288A>.
- 532 [33] C. Mohabeer, L. Reyes, L. Abdelouahed, S. Marcotte, B. Taouk, Investigating catalytic de-  
533 oxygenation of cellulose, xylan and lignin bio-oils using HZSM-5 and Fe-HZSM-5, *Journal*  
534 *of Analytical and Applied Pyrolysis*. 137 (2019) 118–127.  
535 <https://doi.org/10.1016/j.jaap.2018.11.016>.
- 536 [34] T.R. Carlson, J. Jae, Y.-C. Lin, G.A. Tompsett, G.W. Huber, Catalytic fast pyrolysis of  
537 glucose with HZSM-5: The combined homogeneous and heterogeneous reactions, *Journal*  
538 *of Catalysis*. 270 (2010) 110–124. <https://doi.org/10.1016/j.jcat.2009.12.013>.
- 539 [35] C. Liu, H. Wang, A.M. Karim, J. Sun, Y. Wang, Catalytic fast pyrolysis of lignocellulosic  
540 biomass, *Chemical Society Reviews*. 43 (2014) 7594–7623.  
541 <https://doi.org/10.1039/C3CS60414D>.
- 542 [36] S. Wang, G. Dai, H. Yang, Z. Luo, Lignocellulosic biomass pyrolysis mechanism: A state-  
543 of-the-art review, *Progress in Energy and Combustion Science*. 62 (2017) 33–86.  
544 <https://doi.org/10.1016/j.pecs.2017.05.004>.
- 545 [37] Y.-T. Cheng, G.W. Huber, Production of targeted aromatics by using Diels–Alder classes  
546 of reactions with furans and olefins over ZSM-5, *Green Chem*. 14 (2012) 3114.  
547 <https://doi.org/10.1039/c2gc35767d>.
- 548 [38] C.M. Lok, J. Van Doorn, G. Aranda Almansa, Promoted ZSM-5 catalysts for the  
549 production of bio-aromatics, a review, *Renewable and Sustainable Energy Reviews*. 113  
550 (2019) 109248. <https://doi.org/10.1016/j.rser.2019.109248>.
- 551 [39] Nishu, R. Liu, Md.M. Rahman, M. Sarker, M. Chai, C. Li, J. Cai, A review on the catalytic  
552 pyrolysis of biomass for the bio-oil production with ZSM-5: Focus on structure, *Fuel*  
553 *Processing Technology*. 199 (2020) 106301. <https://doi.org/10.1016/j.fuproc.2019.106301>.
- 554 [40] A.M. Hernández- Giménez, E. Heracleous, E. Pachatouridou, A. Horvat, H. Hernando,  
555 D.P. Serrano, A.A. Lappas, P.C.A. Bruijninx, B.M. Weckhuysen, Effect of Mesoporosity,  
556 Acidity and Crystal Size of Zeolite ZSM- 5 on Catalytic Performance during the Ex- situ  
557 Catalytic Fast Pyrolysis of Biomass, *ChemCatChem*. 13 (2021) 1207–1219.  
558 <https://doi.org/10.1002/cctc.202001778>.
- 559 [41] S. Chu, A.V. Subrahmanyam, G.W. Huber, The pyrolysis chemistry of a  $\beta$ -O-4 type  
560 oligomeric lignin model compound, *Green Chemistry*. 15 (2013) 125–136.  
561 <https://doi.org/10.1039/C2GC36332A>.

- 562 [42] H. Ben, A.J. Ragauskas, Influence of Si/Al Ratio of ZSM-5 Zeolite on the Properties of  
563 Lignin Pyrolysis Products, *ACS Sustainable Chemistry & Engineering*. 1 (2013) 316–324.  
564 <https://doi.org/10.1021/sc300074n>.
- 565 [43] S. Tan, Z. Zhang, J. Sun, Q. Wang, Recent progress of catalytic pyrolysis of biomass by  
566 HZSM-5, *Chinese Journal of Catalysis*. 34 (2013) 641–650. [https://doi.org/10.1016/S1872-2067\(12\)60531-2](https://doi.org/10.1016/S1872-2067(12)60531-2).
- 567 [44] M. Carrier, M. Windt, B. Ziegler, J. Appelt, B. Saake, D. Meier, A. Bridgwater,  
568 Quantitative Insights into the Fast Pyrolysis of Extracted Cellulose, Hemicelluloses, and  
569 Lignin, *ChemSusChem*. 10 (2017) 3212–3224. <https://doi.org/10.1002/cssc.201700984>.
- 570 [45] I. Lüderwald, F. Merz, M. Rothe, Über den thermischen abbau des poly-ε-caprolactams  
571 (Nylon-6), *Die Angewandte Makromolekulare Chemie*. 67 (1978) 193–202.  
572 <https://doi.org/10.1002/apmc.1978.050670114>.
- 573 [46] S. Czernik, C.C. Elam, R.J. Evans, R.R. Meglen, L. Moens, K. Tatsumoto, Catalytic  
574 pyrolysis of nylon-6 to recover caprolactam, *Journal of Analytical and Applied Pyrolysis*.  
575 46 (1998) 51–64. [https://doi.org/10.1016/S0165-2370\(98\)00068-0](https://doi.org/10.1016/S0165-2370(98)00068-0).
- 576 [47] H. Bockhorn, A. Hornung, U. Hornung, J. Weichmann, Kinetic study on the non-catalysed  
577 and catalysed degradation of polyamide 6 with isothermal and dynamic methods,  
578 *Thermochimica Acta*. 337 (1999) 97–110. [https://doi.org/10.1016/S0040-6031\(99\)00151-3](https://doi.org/10.1016/S0040-6031(99)00151-3).
- 579 [48] H. Bockhorn, S. Donner, M. Gernsbeck, A. Hornung, U. Hornung, Pyrolysis of polyamide  
580 6 under catalytic conditions and its application to reutilization of carpets, *Journal of*  
581 *Analytical and Applied Pyrolysis*. 58–59 (2001) 79–94. [https://doi.org/10.1016/S0165-2370\(00\)00187-X](https://doi.org/10.1016/S0165-2370(00)00187-X).
- 582 [49] F. Kubatovics, M. Blazsó, Thermal decomposition of polyamide-6 in the presence of PVC,  
583 *Macromolecular Chemistry and Physics*. 201 (2000) 349–354.  
584 [https://doi.org/10.1002/\(SICI\)1521-3935\(20000201\)201:3<349::AID-](https://doi.org/10.1002/(SICI)1521-3935(20000201)201:3<349::AID-MACP349>3.0.CO;2-Y)  
585 [MACP349>3.0.CO;2-Y](https://doi.org/10.1002/(SICI)1521-3935(20000201)201:3<349::AID-MACP349>3.0.CO;2-Y).
- 586 [50] H. Ohtani, T. Nagaya, Y. Sugimura, S. Tsuge, Studies on thermal degradation of aliphatic  
587 polyamides by pyrolysis-glass capillary chromatography, *Journal of Analytical and Applied*  
588 *Pyrolysis*. 4 (1982) 117–131. [https://doi.org/10.1016/0165-2370\(82\)80003-X](https://doi.org/10.1016/0165-2370(82)80003-X).
- 589  
590  
591